

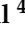





## Article

# Promising Natural Compounds against Flavivirus Proteases: Citrus Flavonoids Hesperetin and Hesperidin

Raphael J. Eberle <sup>1,2,\*</sup> , Danilo S. Olivier <sup>3</sup> , Marcos S. Amaral <sup>4</sup> , Dieter Willbold <sup>1,2,5</sup> , Raghuvir K. Arni <sup>6</sup>   
and Monika A. Coronado <sup>1,\*</sup> 

- <sup>1</sup> Institute of Biological Information Processing (IBI-7: Structural Biochemistry), Forschungszentrum Jülich, 52428 Jülich, Germany; D.Willbold@fz-juelich.de  
<sup>2</sup> Institut für Physikalische Biologie, Heinrich-Heine-Universität Düsseldorf, Universitätsstraße, 40225 Düsseldorf, Germany  
<sup>3</sup> Integrated Sciences Center, Federal University of Tocantins, Araguaína 77824-838, Brazil; doliviercg@gmail.com  
<sup>4</sup> Institute of Physics, Federal University of Mato Grosso do Sul, Campo Grande 79070-900, Brazil; marcosamaral@gmail.com  
<sup>5</sup> JuStruct: Jülich Centre for Structural Biology, Forschungszentrum Jülich, 52428 Jülich, Germany  
<sup>6</sup> Multiuser Center for Biomolecular Innovation, Department of Physics, Universidade Estadual Paulista (UNESP), São Jose do Rio Preto 15054-000, Brazil; raghuvir.arni@unesp.br  
\* Correspondence: r.eberle@fz-juelich.de (R.J.E.); m.coronado@fz-juelich.de (M.A.C.)

**Abstract:** Ubiquitous in citrus plants, Hesperidin and Hesperetin flavanones possess several biological functions, including antiviral activity. Arbovirus infections pose an ever-increasing threat to global healthcare systems. Among the severe arboviral infections currently known are those caused by members of the Flavivirus genus, for example, Dengue Virus—DENV, Yellow Fever Virus—YFV, and West Nile Virus—WNV. In this study, we characterize the inhibitory effect of Hesperidin and Hesperetin against DENV2, YFV, and WNV NS2B/NS3 proteases. We report the noncompetitive inhibition of the NS2B/NS3<sup>PRO</sup> by the two bioflavonoids with half maximal inhibitory concentration (IC<sub>50</sub>) values <5 μM for HST and <70 μM for HSD. The determined dissociation constants (K<sub>D</sub>) of both flavonoids is significantly below the threshold value of 30 μM. Our findings demonstrate that a new generation of anti-flavivirus drugs could be developed based on selective optimization of both molecules.

**Keywords:** hesperetin; hesperidin; flavivirus; NS2B/NS3<sup>PRO</sup>; noncompetitive inhibitors



**Citation:** Eberle, R.J.; Olivier, D.S.; Amaral, M.S.; Willbold, D.; Arni, R.K.; Coronado, M.A. Promising Natural Compounds against Flavivirus Proteases: Citrus Flavonoids Hesperetin and Hesperidin. *Plants* **2021**, *10*, 2183. <https://doi.org/10.3390/plants10102183>

Academic Editor: Daniel K. Owens

Received: 27 September 2021

Accepted: 13 October 2021

Published: 14 October 2021

**Publisher's Note:** MDPI stays neutral with regard to jurisdictional claims in published maps and institutional affiliations.



**Copyright:** © 2021 by the authors. Licensee MDPI, Basel, Switzerland. This article is an open access article distributed under the terms and conditions of the Creative Commons Attribution (CC BY) license (<https://creativecommons.org/licenses/by/4.0/>).

## 1. Introduction

Polyphenols are plant secondary metabolites that are encountered in fruits, vegetables, and seeds that are constituents of normal diet [1]. They occur widely in nature, and to date, more than 9000 flavonoids have been identified [2]; these include, but are not limited to, phenolic acids, coumarins, flavonoids, stilbenes, and lignans [3]. They are characterized by the presence of at least two phenolic groups associated in a complex structure. The wide spectrum of physiological functions exhibited by flavonoids includes antiviral/bacterial, anti-inflammatory, cardioprotective, antidiabetic, anticancer, and antiaging activities [4–7].

Both bioflavonoids HSD and HST are encountered in citrus fruits. Hesperidin (HSD) (3',5,7-trihydroxy-4'-methoxy-flavanone-7-rhamnoglucoside) is a flavanone glycoside (flavonoid subclass) that consist of an aglycone, HST, and a disaccharide rutinose (Figure 1). Hesperetin (HST) (3',5,7-trihydroxy-4'-methoxyflavanone) is its aglycone form [8].

Both flavonoids show antiviral activity and have been reported to inhibit the intracellular replication of Chikungunya and Sindbis viruses [9,10]. Recently, we showed the potential for HST and HSD to be used against Zika and Chikungunya virus proteases (ZIKV and CHIKV) [11].

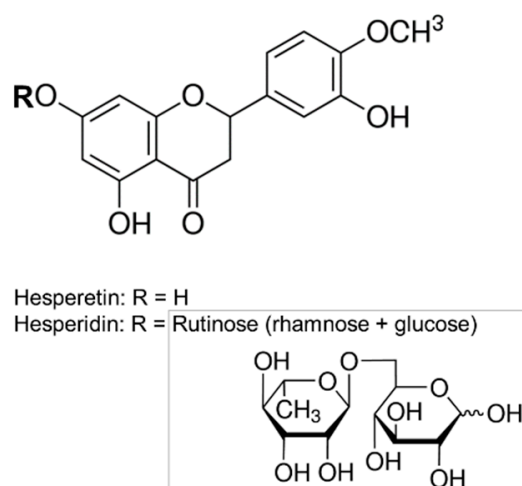


**Figure 1.** The chemical structures of Hesperetin and Hesperidin. The grey box shows the chemical structure of Rutinose.

Factors including urbanization, climate and ecological changes, and unsustainable vector control, make the diseases caused by arthropode transmitted viruses (arboviruses) more prevalent; therefore, they are becoming another emerging threat to global health and welfare [12,13]. Members of the Flavivirus genus cause the most severe arbovirus infections. The genus includes major human pathogens such as Yellow Fever virus (YFV), Dengue virus (DENV), Japanese encephalitis virus (JEV), tick-borne encephalitis virus (TBEV), and West Nile virus (WNV) [14–16]. Flaviviruses are single-stranded, positive-sense RNA viruses, whose genome encodes a polyprotein that can be co- and post-translationally cleaved into three distinct structural proteins and seven nonstructural (NS) proteins (NS1, NS2A, NS2B, NS3, NS4A, NS4B, and NS5) [17]. Important for the proteolytically procession of the polyprotein is the viral protease NS3 [18], which requires the NS2B cofactor for optimal enzymatic activity [19]. The flavivirus replication route is dependent on the NS2B/NS3 protease (NS2B/NS3<sup>pro</sup>), which represents a potential drug target against flavivirus infections [20,21].

Based on our previous findings on the inhibitory effect HST on ZIKV NS2B/NS3<sup>pro</sup>, we hypothesized that the HST and HSD molecules should also exert a similar inhibition of the NS2B/NS3 proteases of DENV2, YFV, and WNV. This hypothesis led us to believe that these molecules could be used as lead molecules in the development of a broad-spectrum antiviral. A fluorogenic inhibition assay demonstrated that HST inhibited the proteases with half-maximal inhibitory concentration (IC<sub>50</sub>) values in the low  $\mu\text{M}$  range, unlike the inhibition presented by HSD, which presented a IC<sub>50</sub> value ten times higher. The determined dissociation constants (K<sub>D</sub>) for HST and HSD were <30  $\mu\text{M}$  and docking, followed by MD simulations of HST and HSD in a complex with the proteases, suggested a possible inhibition mode of these molecules.

## 2. Results and Discussion

### 2.1. Preparation of Flavivirus Proteases

The target proteins (DENV2, YFV, and WNV NS2B/NS3<sup>pro</sup>) were expressed in *E. coli* Lemo (DE3) cells. The soluble proteases were purified in two steps as follows: Ni-NTA to separate the target protein from *E. coli* proteins followed by subsequent size exclusion chromatography. The purity of the proteases was checked by SDS-PAGE 15% (Supplementary Figure S1A–C).

### 2.2. Inhibition of DENV2, YFV, and WNV Proteases by HST and HSD

Flavonoids and their subgroups comprise structural diversity, which can be used to identify potential inhibitors that can serve as lead compounds for the development of

efficacious and efficient alternatives to combat pathogens [22]. Based on this, we performed a primary inhibitory test using HST and HSD to check their effect against DENV2, YFV, and WNV NS2B/NS3<sup>pro</sup> (Figure 2).

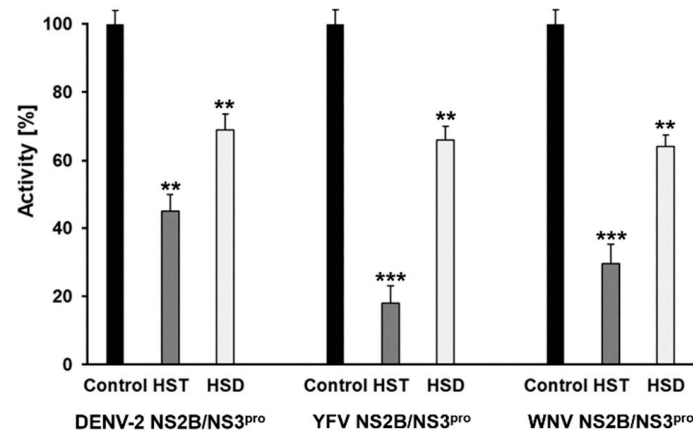


**Figure 2.** Primary inhibition test using HST and HSD as inhibitor molecules against flavivirus proteases. DENV2, YFV, and WNV NS2B/NS3<sup>pro</sup> enzymatic activity [%]. Final concentration of the compound was set to 10  $\mu$ M. HST inhibited the proteases activity between 55% and 80%. Contrary to this, HSD inhibited the proteases activity by about 30%. The data shown are the mean  $\pm$  SD from 3 independent measurements ( $n = 3$ ). Asterisks mean that the data differs from the control (0  $\mu$ M inhibitor) significantly at  $p < 0.01$  (\*\*) and  $p < 0.001$  (\*\*\*), level according to ANOVA and Tukey's test.

An amount of 10  $\mu$ M of HST inhibited the DENV2 NS2B/NS3<sup>pro</sup> activity by around 55%, the YFV NS2B/NS3<sup>pro</sup> (~80%), and the WNV NS2B/NS3<sup>pro</sup> (~70%). In contrast, 10  $\mu$ M of HSD shows inhibition of the three tested proteases to be around 30%.

For further information of the inhibitory effects of both flavonoids, new experiments were carried out. To evaluate the effect of HST against the described viral proteases, the concentration range of 0–140  $\mu$ M (DENV2) and 0–100 mM (YFV, WNV) were tested (Figure 3).

HST inhibited 100% of the DENV2 protease activity at a concentration of 140  $\mu$ M (Figure 2A), and the activity of the YFV and WNV NS2B/NS3<sup>pro</sup> were inhibited completely at a concentration of 80  $\mu$ M (Figure 2C,E). The calculated IC<sub>50</sub> values for HST and the virus proteases NS2B/NS3<sup>pro</sup> are  $< 5 \mu$ M, DENV2 ( $4.7 \pm 0.8 \mu$ M), YFV ( $2.0 \pm 0.5 \mu$ M), and WNV ( $4.3 \pm 1.6 \mu$ M) (Table 1 and Supplementary Figure S2A–C).

On the contrary, HSD inhibited the DENV2 and YFV protease activity by 100% at a concentration of 140  $\mu$ M (Figure 4A,C), and the WNV protease was inhibited completely at a final concentration of 120  $\mu$ M (Figure 3E), showing a probable steric effect of the sugar group. The calculated IC<sub>50</sub> values for HSD and the virus proteases NS2B/NS3<sup>pro</sup> are between 50 and 70  $\mu$ M: DENV2 ( $55.7 \pm 2.5 \mu$ M), YFV ( $67.7 \pm 7.5 \mu$ M), and WNV ( $50.7 \pm 8.3 \mu$ M) (Table 1 and Supplementary Figure S2D–F).

Further experiments identified HST and HSD as noncompetitive inhibitors (Table 1 and Figures 3 and 4B,D,F), as was described previously for ZIKV NS2B/NS3<sup>pro</sup> [11]. As noncompetitive inhibitors, HST and HSD show a type of allosteric inhibition.

When a noncompetitive inhibitor is added, the maximum rate ( $V_{max}$ ) values for the flavivirus NS2B/NS3 proteases were changed, when in the presence of HST and HSD at various concentrations; whereas, the Michaelis–Menten constant ( $K_M$ ) remains unaltered, which is shown on the Lineweaver–Burk plot by a change in the slope and y-intercept (see Figures 3 and 4). In contrast, a competitive inhibitor would not affect the  $V_{max}$  values but would increase the  $K_M$  values [23].

We have previously reported that the IC<sub>50</sub> value of HST for ZIKV NS2B/NS3<sup>pro</sup> [11]—another flavivirus protease—was  $12.6 \pm 1.3 \mu$ M, which is in the same concentration range as the determined IC<sub>50</sub> values of HST for DENV2, YFV, and WNV NS2B/NS3<sup>pro</sup> (Table 1). The inhibitory effect of HSD against ZIKV NS2B/NS3<sup>pro</sup> was not further investigated.

The inhibitory effect of bioactive flavonoids against flavivirus NS2B/NS3 proteases have already been described; furthermore, the  $IC_{50}$  values of our results by both molecules were in the same  $\mu\text{M}$  range as demonstrated by other flavonoids [11,24–26].

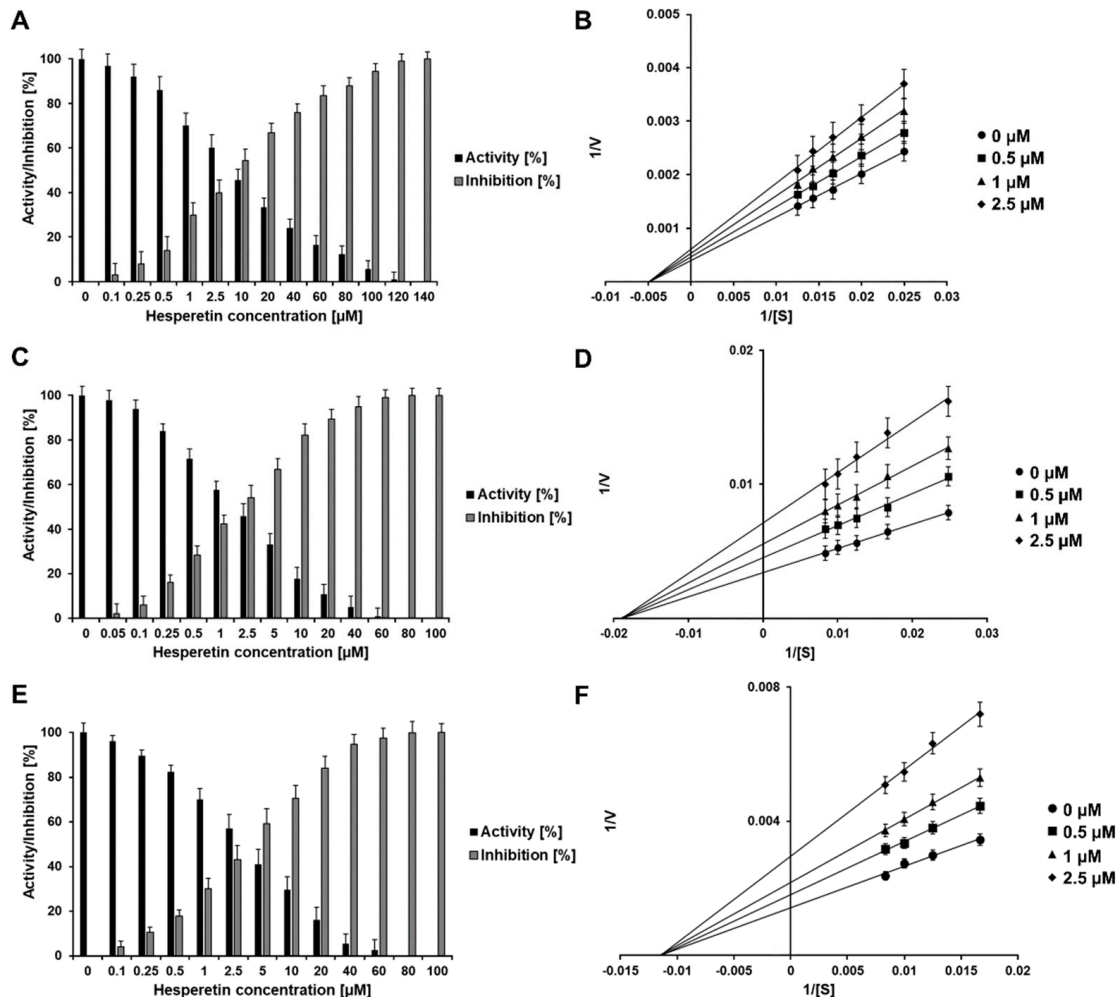


**Figure 3.** Normalized activity, inhibition effect and inhibition mode of HST over DENV2, YFV, and WNV NS2B/NS3<sup>PRO</sup>. Lineweaver-Burk plots were used to determine the inhibition modes. [S] is the substrate concentration;  $v$  is the initial reaction rate. Inhibition of DENV2, YFV, and WNV NS2B/NS3<sup>PRO</sup> by HST are shown in (A,C,E), respectively. Lineweaver-Burk plots for HST inhibition of DENV2, YFV, and WNV NS2B/NS3<sup>PRO</sup> are shown in (B,D,F), respectively. Data shown are the mean  $\pm$  SD from 3 independent measurements ( $n = 3$ ).

**Table 1.** Inhibitor key numbers and inhibition modes of HST and HSD for DENV2, YFV, WNV, and ZIKV NS2B/NS3<sup>PRO</sup>.

Protease	Molecule	$IC_{50}$ <sup>a</sup>	Inhibition Mode	$pIC_{50}$ <sup>b</sup>	LE <sup>c</sup>	N <sup>d</sup>	Reference
DENV2 NS2B/NS3 <sup>PRO</sup>	HST	$4.7 \pm 0.8$	noncompetitive	5.33	0.34	22	
	HSD	$55.7 \pm 2.5$	noncompetitive	4.25	0.14	43	
YFV NS2B/NS3 <sup>PRO</sup>	HST	$2.0 \pm 0.5$	noncompetitive	5.69	0.36	22	
	HSD	$67.7 \pm 7.5$	noncompetitive	4.17	0.13	43	
WNV NS2B/NS3 <sup>PRO</sup>	HST	$4.3 \pm 1.6$	noncompetitive	5.37	0.34	22	
	HSD	$50.7 \pm 8.3$	noncompetitive	4.29	0.14	43	
ZIKV NS2B/NS3 <sup>PRO</sup>	HST	$12.6 \pm 1.3$	noncompetitive	4.90	0.31	22	[11]
	HSD <sup>e</sup>	-	-	-	-	-	[11]

<sup>a</sup>  $IC_{50}$  value  $\pm$  STD in  $\mu\text{M}$ . <sup>b</sup> Logarithm of  $IC_{50}$  value ( $pIC_{50}$ ). <sup>c</sup> Ligand efficiency (LE): LE > 0.3 suggests that the molecule is a potent lead compound. <sup>d</sup> Number of non-hydrogen atoms (N). <sup>e</sup> HSD was not further investigated in Eberle et al., 2021 [11].

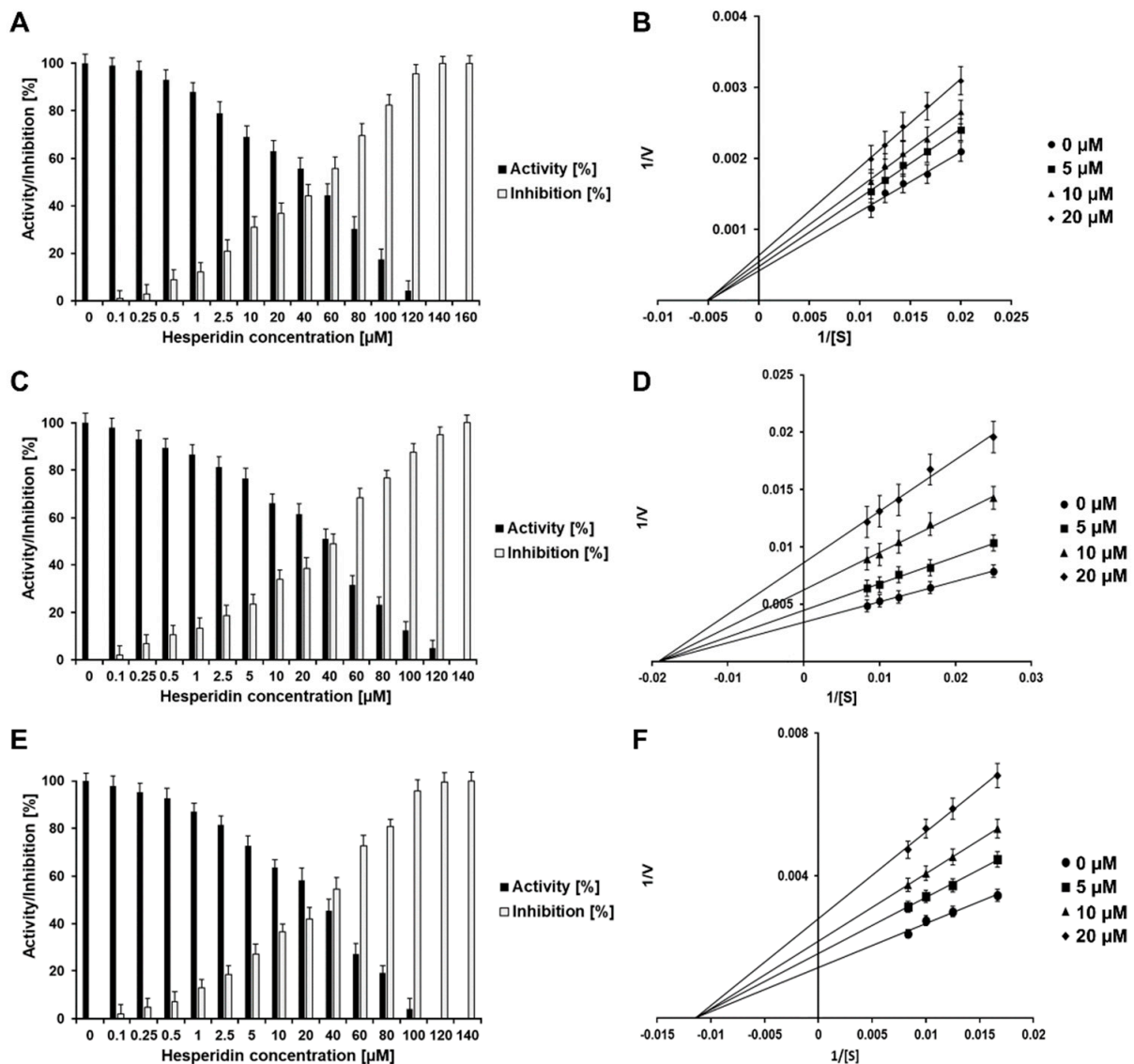


**Figure 4.** Normalized activity, inhibition effect and inhibition mode of HSD over DENV2, YFV, and WNV NS2B/NS3<sup>PRO</sup>. Lineweaver-Burk plots were used to determine the inhibition mode of HSD. [S] is the substrate concentration;  $v$  is the initial reaction rate. Inhibition of DENV2, YFV, and WNV NS2B/NS3<sup>PRO</sup> by HSD are shown in (A,C,E), respectively. Lineweaver-Burk plot for HSD inhibition of DENV2 NS2B/NS3<sup>PRO</sup>. Inhibition of YFV NS2B/NS3<sup>PRO</sup> by HSD is shown in (B,D,F). Data shown are the mean  $\pm$  SD from 3 independent measurements ( $n = 3$ ).

The measurement of ligand efficiency (LE) is a widely used tool for selecting leads for further improvement and development in examining the relationships between inhibitory potential, ligand binding affinity, and molecular size [27,28]. HST possesses LE values  $> 0.30$ , which indicates it to be an efficient binder to the tested virus proteases [27], with the potential to be used as a lead compound for further improvement and development of a broad-spectrum antiviral to fight flavivirus infections targeting the NS2B/NS3 protease. On the contrary, the LE values for HSD are below the method limit, which may depend on the size of the ligand (this has already been described in the literature) [28]. Our findings demonstrated that HST was the compound that consistently showed significant activity against all three tested virus proteases. The increased values of  $IC_{50}$  for HSD demonstrated the direct effect of the sugar moiety presented in the molecule. LE values clearly demonstrated the efficacy of HST as a lead compound against the studied flaviviruses.

### 2.3. DENV2, YFV, and WNV NS2B/NS3<sup>pro</sup>–HST and HSD Interaction, as Determined by TFS

TFS (tryptophan fluorescence spectroscopy) was used to characterize the studied viral proteases binding to HST and HSD. The viral proteases contain five (DENV2), seven (YFV), and six (WNV) tryptophan residues in the NS2B cofactor domain and in the NS3 protease domain. The maximum of the tryptophan fluorescence emission peak of the NS2B/NS3<sup>pro</sup> occurred in ranges 350–361 nm (DENV2), 336–358 (YFV), and 340–355 (WNV), respectively, after titration with HST (Supplementary Figure S3). Titration of the increasing amount of HST resulted in a red edge excitation shift (REES) of 11, 22, and 15 nm, respectively, of the proteases maximum fluorescence peaks to a lower wavelength. Increasing interactions between tryptophan and the surrounding solvent is characteristic for REES [29]. On the contrary, HSD interaction induced no shift of the fluorescence maximum (Supplementary Figure S6B).

The results of the TFS experiments allowed us to determine the  $K_D$  values of the proteases–flavonoid interaction (Supplementary Figures S3 and S4). The calculated  $K_D$  values are summarized in Table 2. A similar binding strength between YFV and WNV NS2B/NS3<sup>pro</sup> and HST could be observed ( $12.3 \pm 2.2 \mu\text{M}$  and  $13.5 \pm 2.0 \mu\text{M}$ , respectively). The difference to the  $K_D$  value for the DENV2 NS2B/NS3<sup>pro</sup>–HST interaction is marginal at  $18.7 \pm 2.7 \mu\text{M}$ . The  $K_D$  values are similar to the ZIKV NS2B/NS3<sup>pro</sup>–HST interaction described previously ( $17.8 \pm 2.9$ ) [11].

**Table 2.**  $K_D$  values of HST and HSD with DENV2, YFV, WNV, and ZIKV NS2B/NS3<sup>pro</sup>, as determined by TFS.

Protease	Molecule	$K_D$ <sup>a</sup>	References
DENV2 NS2B/NS3 <sup>pro</sup>	HST	$18.7 \pm 2.7$	
	HSD	$20.9 \pm 2.4$	
YFV NS2B/NS3 <sup>pro</sup>	HST	$12.3 \pm 2.2$	
	HSD	$29.5 \pm 2.8$	
WNV NS2B/NS3 <sup>pro</sup>	HST	$13.5 \pm 2.0$	
	HSD	$19.5 \pm 2.8$	
ZIKV NS2B/NS3 <sup>pro</sup>	HST	$17.8 \pm 2.9$	[11]
	HSD <sup>b</sup>	-	[11]

<sup>a</sup>  $K_D$  value  $\pm$  STD in  $\mu\text{M}$ . <sup>b</sup> HSD was not further investigated in Eberle et al., 2021.

The  $K_D$  value for the HSD interaction with DENV2 NS2B/NS3<sup>pro</sup> is similar to the HST  $K_D$  (Table 2). In the cases of YFV and WNV NS2B/NS3<sup>pro</sup>, the HSD values increase to about factor 1.4 and 2.4, compared with HST (Table 2).

The NS2B/NS3 proteases of DENV2, YFV, and WNV share high sequences and structural similarities, as well as demonstrating a similar binding specificity towards HST. The increased values of  $K_D$  for the binding of HSD is probably due to the difference in its ability to accommodate the sugar moiety.

### 2.4. In Silico Studies of the Proteases–Flavonoids Interaction

Prior to performing molecular docking, we carried out 200 ns of MD simulation of the single experimental models of DENV2 NS2B/NS3<sup>pro</sup> (PDB entry: 4M9T), YFVNS2B/NS3<sup>pro</sup> (PDB entry: 6URV), and WNV NS2B/NS3<sup>pro</sup> (PDB entry: 2FP7). The flexibility of the protease structures of the MD simulation system was monitored by calculating the RMSD, RMSF, RoG, and the surface area (Supplementary Figures S5–S7). During the simulation of the DENV2, YFV, and WNF NS3<sup>pro</sup> structures, the C $\alpha$  RMSD for NS3<sup>pro</sup> was below 3.5 Å for most of the simulation time. This was also the case for YFV and WNV NS2B structures, unlike the DENV NS2B C $\alpha$  RMSD, which was about 5 Å. Clearly, the structures undergo some structural changes over the simulation time; however, simulations demonstrated stable structures with 200 ns (Supplementary Figures S5–S7).

In previous work, a hydrophobic allosteric pocket of NS3<sup>pro</sup>, located near the NS2B cofactor interaction area had been mapped for ZIKV NS2B/NS3<sup>pro</sup> [11]. The same area was

assumed for DENV2, YFV, and WNV proteases. Molecular docking and MD simulations of HST and HSD with the virus proteases were performed, aiming to identify a possible allosteric binding area. Therefore, HST and HSD were docked nearby the NS2B cofactor interaction area and two sets of simulations (200 ns each) were performed independently. Based on binding energy and frames in the cluster, a representative structure was chosen for each protease–ligand complex (Table 3).

The ligand–protein complexes analyses—through structural fluctuation—showed stability over the 200 ns of both molecular dynamics simulations as shown for: HST (Supplementary Figures S8–S10) and HSD (Supplementary Figures S11–S13). The position of both flavonoids in the hydrophobic allosteric pocket of NS3<sup>PRO</sup> is demonstrated for all three proteases in Supplementary Figure S14.

Based on energy interactions, further analysis of the MD simulations identified the DENV2, YFV, and WNV NS2B/NS3<sup>PRO</sup> amino acid residues involved in the binding with HST and HSD (Figures 5 and 6). Outstanding in the interaction of the virus proteases with HST is the region surrounding Ile123 (DENV2 and WNV) and Ile126 (YFV). In contrast to DENV2 and YFV NS2B, in the WNV NS2B/NS3<sup>PRO</sup> the residues Leu31 and Phe37 of the NS2B cofactor are involved in the interaction with HST (Figure 5C).

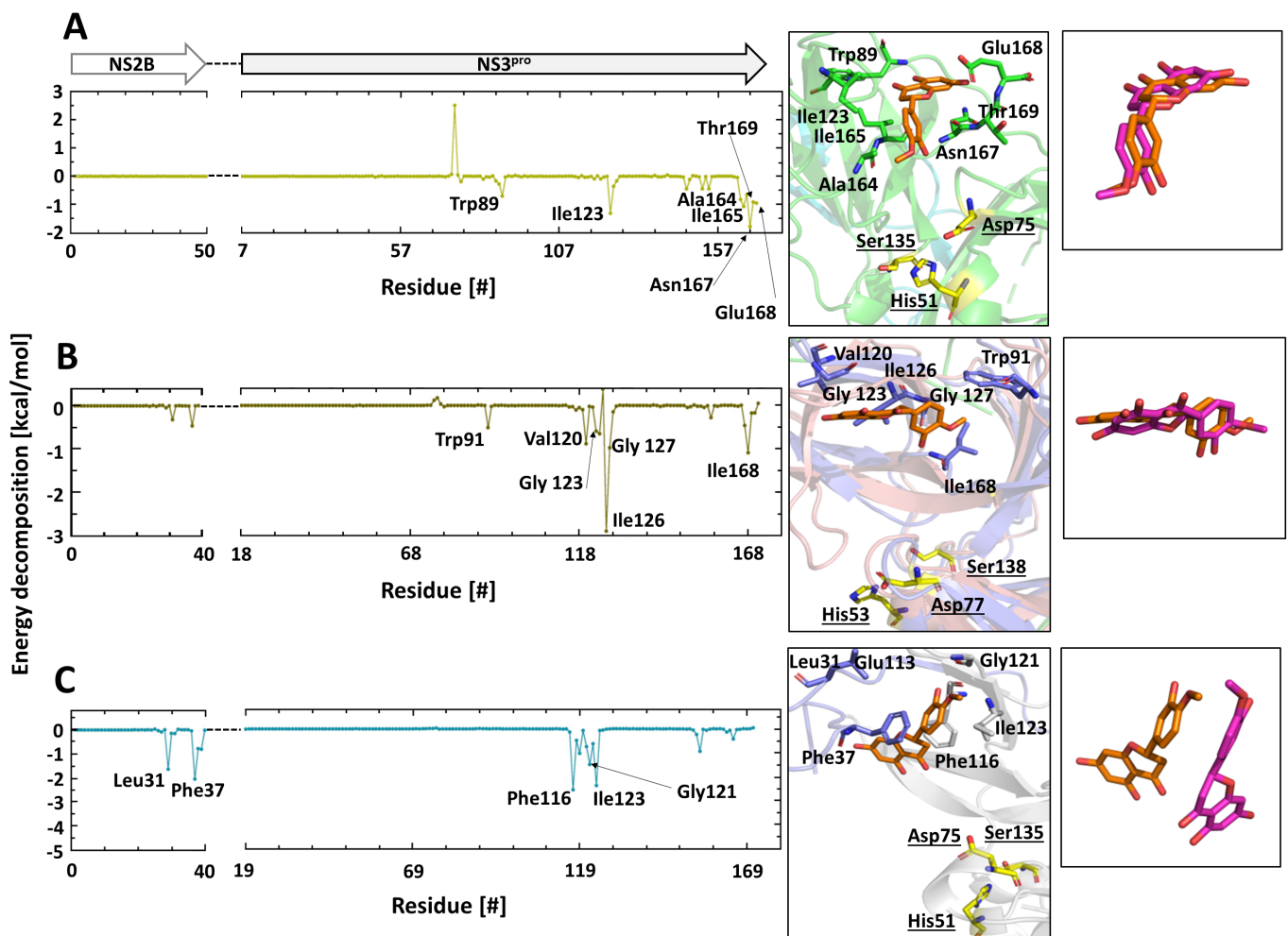


**Figure 5.** Amino acids contributing in the DENV2, YFV, and WNV NS2B/NS3<sup>PRO</sup>–HST interaction. Decomposition energy of the amino acids that participated in the interaction with HST is based on the MD simulations. Coordination of HST in the protease binding region and overlay of the HST replicas 1 and 2: (A) DENV2 NS2B/NS3<sup>PRO</sup>–HST interaction; (B) YFV NS2B/NS3<sup>PRO</sup>–HST interaction; (C) WNV NS2B/NS3<sup>PRO</sup>–HST interaction. Amino acid residues with an energy decomposition < −1 kcal/mol are considered.

The two independent MD simulation replicas demonstrate a very similar location for HST in DENV2 and YFV NS2B/NS3<sup>pro</sup>. It is important to mention that the molecule was in the same starting poses; however, they had different velocities that implied different energies. The interacting amino acid residues were all the same, showing only minor intensity changes in energy due to statistical fluctuations along the trajectory (Figure 5A,B, and Supplementary Figures S15 and S16). Contrary to this, during the MD simulation replicas of HST with the WNV protease, some fluctuations could be observed over time (Figure 5C and Supplementary Figure S17).

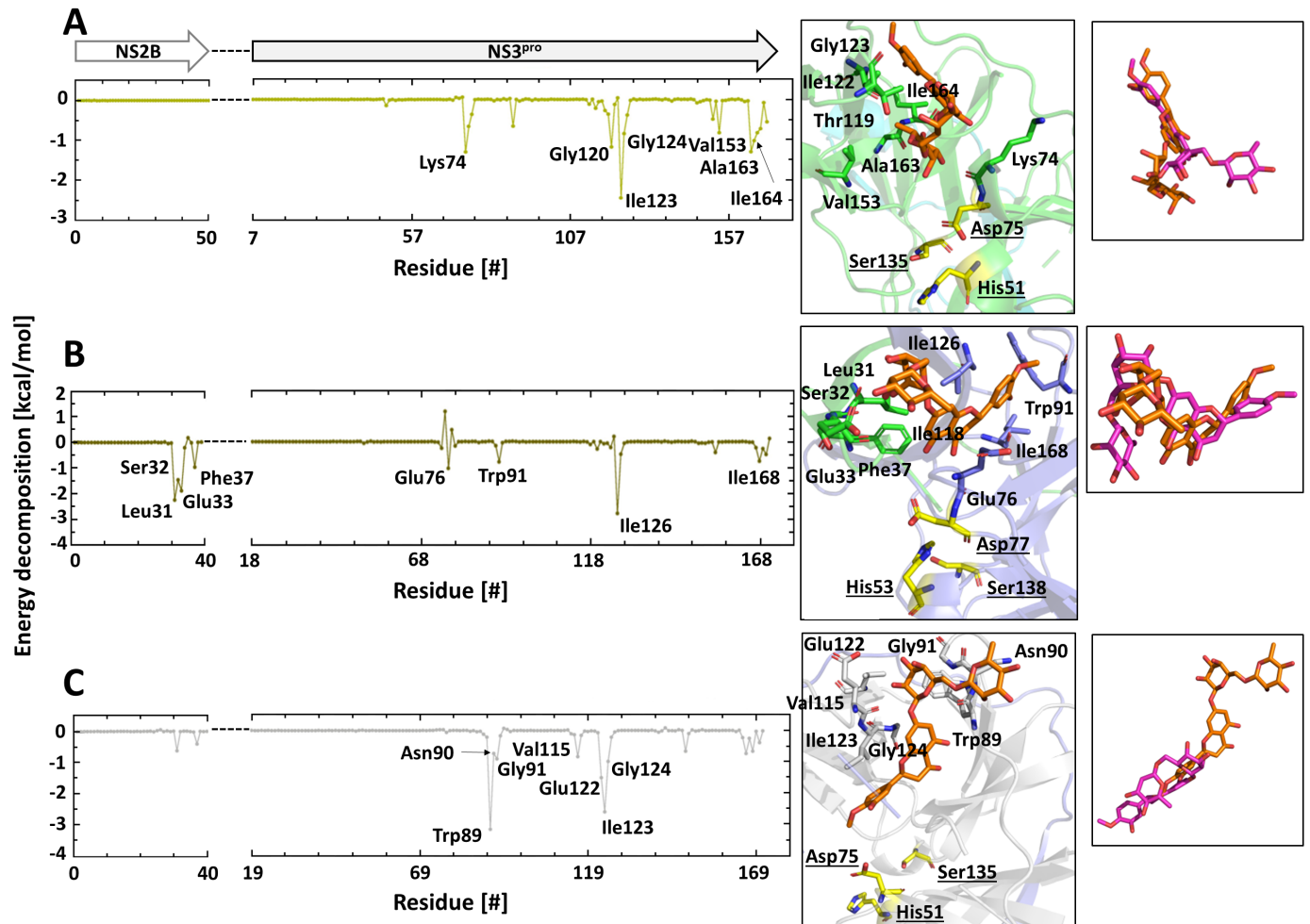


**Figure 6.** Amino acids contributing to the DENV2, YFV, and WNV NS2B/NS3<sup>pro</sup>–HSD interaction. The decomposition energies of amino acids that participated in the interaction with HSD are based on the MD simulations. Coordination of HSD in the protease binding region and overlay of the HSD replicas 1 and 2; (A) DENV2 NS2B/NS3<sup>pro</sup>–HSD interaction; (B) YFV NS2B/NS3<sup>pro</sup>–HSD interaction; (C) WNV NS2B/NS3<sup>pro</sup>–HSD interaction. Amino acid residues with an energy decomposition <math>< -1</math> kcal/mol are considered.

Similarly to HST, the surrounding areas of Ile123 (DENV2 and WNV) and Ile126 (YFV) were involved in the interaction with HSD, and the Ile residue showed mostly the strongest binding energy (Figure 6). In the YFV NS2B, four amino acid residues could be identified that stabilized the interaction with HSD (Leu31, Ser32, Glu33, and Phe37) (Figure 5B and Supplementary Figures S18–S20). Moreover, this region is involved in the WNV NS2B–HST interaction (Figure 5C).

The results of the two MD replicas of the protease–HSD complexes demonstrated that the fluctuation of HSD was much more dynamic when compared with the results presented by HST. The fluctuation of the sugar moiety (rutinose) demonstrates that it is not involved



in a stable interaction with the proteases, e.g., a hydrogen bond. However, the results of the two independent runs of MD simulations allow us to assume that the regions surrounding Ile123 (DENV2 and WNV) and Ile126 (YFV) forms a potential allosteric binding site for HST and minor HSD. In our previous results with the ZIKV NS2B/NS3<sup>PRO</sup>-HST complex, the MD simulations demonstrated the residues Leu31, Phe37, and Ile24 interacting with HST [11], which is in agreement with the presented results.

**Table 3.** Summary of the MD simulation replicas 1 and 2 of DENV2, YFV and WNV NS2B/NS3<sup>PRO</sup> in complex (with HST and HSD molecules).

Protein + Ligand	Replicate	Binding Energy [kcal/mol]	Representative Frames Cluster [%]
DENV2 NS2B/NS3 <sup>PRO</sup> -HST	1	<b>-23.1 ± 3.6</b>	<b>68.9</b>
	2	-24.1 ± 3.7	62.0
YFV NS2B/NS3 <sup>PRO</sup> -HST	1	-20.0 ± 3.4	54.9
	2	<b>-19.4 ± 2.7</b>	<b>64.8</b>
WNV NS2B/NS3 <sup>PRO</sup> -HST	1	-20.2 ± 3.4	72.7
	2	<b>-28.3 ± 3.0</b>	<b>90.3</b>
DENV2 NS2B/NS3 <sup>PRO</sup> -HSD	1	<b>-37.4 ± 7.2</b>	<b>95.3</b>
	2	-38.6 ± 8.0	75.0
YFV NS2B/NS3 <sup>PRO</sup> -HSD	1	-35.4 ± 5.2	36.9
	2	<b>-37.6 ± 6.2</b>	<b>75.7</b>
WNV NS2B/NS3 <sup>PRO</sup> -HSD	1	<b>-40.7 ± 4.7</b>	<b>63.1</b>
	2	-37.8 ± 7.0	54.2

Chosen representative protease–ligand structure in bold.

### 3. Materials and Methods

#### 3.1. Cloning of DENV2, YFV, and WNV Proteases

DENV2 and WNV NS2B/NS3<sup>PRO</sup> constructs were provided by Prof. Rolf Hilgenfeld, University Lübeck, Germany. The cDNA encoding DENV2 and WNV NS2B/NS3<sup>PRO</sup> (GenBank Protein Accession number AHZ13508.1 and AAA48498.2) were synthesized and implemented in the ampicillin resistant vector pET-15b (+) (Fisher Scientific Geneart, Regensburg, Germany).

YFV NS2B/NS3<sup>PRO</sup> cDNA (GenBank Protein Accession number AAY34247.1, isolate Angola/14FA/1971) was codon optimized, synthesized (BioCat GmbH, Heidelberg, Germany), and implemented in the kanamycin resistant vector pET-24a (+).

The construct contains the NS2B cofactor region (DENV2: residues 49–96; YFV: 48–96; WNV: 52–96) linked with NS3 protein (DENV2 residues 1–178; YFV: 1–191; WNV: 1–184). Both domains are connected by a G4SG4 linker. The constructs contain an N-terminal hexahistidine affinity tag and a TEV proteinase cleavage site (ENLYFQG).

#### 3.2. Heterologous Gene Expression and Purification of the Virus Proteases

The virus NS2B/NS3 plasmids of DENV2 (pET-15b (+)), YFV (pET-24a (+)), and WNV (pET-15b (+)) were transformed into Lemo (DE3) *E. coli* competent cells (New England BioLabs, Ipswich, MA, USA), which were cultured overnight in LB medium at 37 °C in the presence of appropriate antibiotics according to the vector. Upon reaching an optical density of ~0.8 at 600 nm, protein expression was induced by adding Isopropylthiogalactoside. Cells were harvested, lysed, and centrifuged at 8000 rpm for 90 min. The supernatant was collected and applied to an affinity column using immobilized metal (Ni-NTA). The target protein was eluted from 100 mM to 500 mM imidazole buffer. Subsequently, the proteins were further purified with size-exclusion chromatography using a Superdex 75 10/30 column and showed ~95% purity on SDS-PAGE (for detailed information see Supplementary Text S1).

### 3.3. Inhibition Assay of DENV2, YFV, and WNV NS2B/NS3<sup>pro</sup>

The DENV2, YFV, and WNV NS2B/NS3<sup>pro</sup> activity assay was performed as described previously [30–32], using a fluorogenic substrate (Boc-Gly-Arg-Arg-AMC; BACHEM, Bubendorf, Switzerland). This procedure was used to investigate the inhibitory effect of HST (Merck, Darmstadt, Germany, purity > 95%) and HSD (Merck, Darmstadt, Germany, purity > 80%) against the virus proteases. The DENV2 (250 nM), YFV (6 nM), and WNV (50 nM) NS2B/NS3<sup>pro</sup>, separately, were incubated with 0–140  $\mu$ M HST, 0–160  $\mu$ M HSD (DENV2 NS2B/NS3<sup>pro</sup>) and 0–100  $\mu$ M HST, 0–140  $\mu$ M HSD (YFV and WNV NS2B/NS3<sup>pro</sup>) in assay buffer containing 20 mM Tris pH 8.5, 10% glycerol, and 0.01% Triton X-100 and incubated for 1 h at RT.

The inhibition assay was performed in Corning 96-well plates (Merck, Darmstadt, Germany). The measurement started by addition of the substrate with a final concentration of 50  $\mu$ M. The fluorescence intensities were measured at 60 s intervals over 30 min at 37 °C using an Infinite 200 PRO plate reader (Tecan, Männedorf, Switzerland). The excitation and emission wavelengths were 380 nm and 465 nm, respectively. The IC<sub>50</sub> values were calculated using GraphPad Prism5 software (San Diego, CA, USA). All measurements were performed in triplicate, and data are presented as mean  $\pm$  SD.

### 3.4. Characterisation of the Type of Inhibition and LE of HST and HSD

The inhibition mode of HST and HSD for viral proteases was characterized using a modified form of the activity assay described above. DENV2, YFV, and WNV NS2B/NS3<sup>pro</sup> at concentrations of 250 nM, 6 nM, and 50 nM, respectively, were incubated with different concentrations of HST and HSD, separately, for 1 h at RT. The reaction was initiated by the addition of the corresponding concentration series of the substrate and the fluorescence intensities were measured at 60 s intervals over 30 min at 37 °C using an Infinite 200 PRO plate reader (Tecan, Männedorf, Switzerland). A Lineweaver–Burk approach was used to analyse the data, comparing the reciprocal of velocity (1/V) vs. the reciprocal of the substrate concentration (1/[S]) [24,33]. All measurements were performed in triplicate, and data are presented as mean  $\pm$  SD.

The ligand efficiencies for HST and HSD were calculated using Formula (1) as follows [27]:

$$(1.4 \times pIC_{50})/N \quad (1)$$

$pIC_{50}$  was obtained utilizing an online tool [34], and N is the number of all atoms except hydrogen.

### 3.5. Intrinsic Tryptophan Fluorescence Spectroscopy (TFS)

The dissociation constants (K<sub>D</sub>) for HST and HSD in complexes with DENV2, YFV, and WNV NS2B/NS3<sup>pro</sup> were determined using intrinsic tryptophan fluorescence spectroscopy (TFS), as described previously [35]. TFS was measured with a QuantaMaster40 spectrofluorometer (PTI, Birmingham, AL, USA), using 1 cm path length quartz cuvettes (105.253-QS, Hellma, Mühlheim, Germany). To avoid excitation of tyrosin residues, an excitation wavelength at 295 nm was chosen. The emission spectrum was collected in the range of 300–500 nm with the increment 1 nm. Each data point on the emission spectrum is an average of 10 accumulations. The final viral proteases concentration was set to 10  $\mu$ M in a buffer containing 25 mM Tris-HCL, pH 8.5, 150 mM NaCl, and 5% glycerol. The measuring volume was 50  $\mu$ L.

During the interaction measurement, the protein solution within the cuvette was titrated stepwise with a ligand stock solution (0.5 mM ligand + 10  $\mu$ M protein): DENV NS2B/NS3<sup>pro</sup>–HST/HSD (0–70  $\mu$ M); YFV NS2B/NS3<sup>pro</sup>–HST/HSD (0–100  $\mu$ M); WNV NS2B/NS3<sup>pro</sup>–HST/HSD (0–100  $\mu$ M).

The quenching of the protease fluorescence,  $\Delta F (F^{\max} - F)$ , at 337 nm of each titration point was considered and a saturation binding curve was fitted using a nonlinear least squares fit procedure, [36], based on Equation (2) as follows [37]:

$$Y = B_{\max}[Q]/K_D + [Q] \quad (2)$$

where  $[Q]$  is the ligand concentration in solution (quencher),  $Y$  is the specific binding derived by measuring fluorescence intensity,  $B_{\max}$  is the maximum amount of the complex protease–ligand at saturation of the ligand, and  $K_D$  is the equilibrium dissociation constant. The percentage of bound protease (i.e.,  $y$ ) that is derived from the fluorescence intensity maximum is plotted against the ligand concentration.

A modified Hill equation was used to determine the  $K_D$  value, following relation (3) as follows [38,39]:

$$\text{Log} (F - F^{\min})/(F) = m \text{ log } K_D + n \text{ log } [Q] \quad (3)$$

where  $F^{\min}$  is the minimal fluorescence intensity in the presence of the ligand and  $K_D$  is the equilibrium constant for the protein–ligand complex. The “binding constant”  $K$  is defined as the reciprocal of  $K_D$ ,  $m$  is the Hill equation’s coefficient, and  $n$  is the number of occupied binding sites.

### 3.6. Statistical Analysis

Statistical analyses were performed with GraphPad Prism software version 8 (San Diego, CA, USA). The experimental measurements consisted of three independent replications. Data are presented as mean values  $\pm$  standard deviation (SD). Statistical significance was analyzed using one-way ANOVA, followed by Tukey’s multiple comparison test. Significant differences were considered at  $p < 0.05$  (\*),  $p < 0.01$  (\*\*), and  $p < 0.001$  (\*\*\*)

### 3.7. Molecular Dynamics and Computational Analysis

#### 3.7.1. Ligand Parameterization

The ligand structures for HST and HSD were retrieved from the Zinc database [40]. Ligands were parameterized for MD simulation using Gaussian16 [41] at the B3LYP/6–31G\* level of theory. The geometry was optimized, and the electrostatic potentials were calculated. Antechamber [42] was used to determine the restrained electrostatic potential (RESP) charges, and the general amber force field (GAFF) [43] was used for missing parameters.

#### 3.7.2. System Preparation

The viral protease structures were retrieved from the PDB database with the following PDB codes: DENV—4M9T, YFV—6URV, and WNV—2FP7. All proteases, single or in complexes (protease–ligand), were placed in an octahedral box of TIP3P water extended to at least 10 Å of any solute atom. The systems were neutralized with  $\text{Na}^+$  or  $\text{Cl}^-$  ions. The proteins were submitted to H++ web server [44] to adjust the lateral sidechain of the amino acids to simulate at pH 7.4.

#### 3.7.3. Simulation Setup

Amber 18 [45] was used to carry out all MD simulations. Protein interactions were described using the all-atom force field FF19SB [46], while the GAFF and RESP charges were used to describe the ligand molecules. To remove bad contacts from the initial structures, each system was energy minimized in two steps. First, the energy minimization of the restricted protein or complex was performed with 5000 steepest descending steps, followed by 5000 conjugated gradient steps, with a force constant of 10.0 kcal/mol-Å<sup>2</sup>. A second round of unconstrained energy minimization was performed during 10,000 steps. After minimization, the system was heated from 0 to 298 K for 500 ps under constant atom number, volume, and temperature (NVT) ensemble, with proteins constrained with force constant of 10 kcal/mol-Å<sup>2</sup>.

Equilibration processes were performed using constant atom number, pressure, and temperature (NPT) ensemble, divided into six steps with decreasing force constant constraint of the protein or complex atoms from 10 to 0 kcal/mol-Å<sup>2</sup>. Finally, a production run was performed for each system for 200 ns in an NVT ensemble without any restriction. All simulated systems were duplicated. The SHAKE restrictions were applied to all bonds involving hydrogen atoms to allow for a 2 fs dynamic time interval. The long-range electrostatic interactions were calculated using the Ewald particle mesh (PME) method using 8 Å cutoff [47]. Langevin coupling was used to control temperature (298 K) and pressure (1 atm).

#### 3.7.4. Molecular Dynamics Analysis

MD results were analyzed using CPPTRAJ [48] tools of the AmberTools19 [49] package. Equilibration and convergence of the systems (single protein and complexes) were investigated with root-mean-square Deviation (RMSD). To quantify protein flexibility, the root-mean-square Fluctuation (RMSF) of the C $\alpha$  atoms were calculated. Structural changes in the protein structure were evaluated by determination of the radius of gyration (RoG) and surface area.

Representative structures for each simulation were obtained using clustering analysis with a k-means method, ranging from 2 to 6 clusters, while the clustering quality was accessed using the Davies–Bouldin index (DBI) values.

The molecular mechanics/generalized Born surface area (MM/GBSA) was calculated between protein–ligand complexes using the generalized Born (GB)-Neck2 [50] implicit solvent model (igb = 8), in the steady-state regime of the last 100 ns of the simulation time, stripping the solvent and ions.

## 4. Conclusions

Currently, no specific therapy can significantly inhibit infection caused by DENV, YFV, and WNV viruses. Treatment focuses on alleviating symptoms; however, they do not treat the infection itself. Exploring promising antiviral agents remains essential for the cure of flavivirus infection. In this study, we demonstrated that Hesperidin and its aglycone form, Hesperetin—bioactive citrus plant flavonoids—might provide benefits in the development of a new drug to fight DENV2, YFV, and WNV, via inhibition of the NS2B/NS3 protease.

Our results can be considered as a preliminary investigation and specific modifications can increase the relevant pharmaceutical properties of the molecules; for example, specificity towards targets, absorption of molecules into the cell and passage through the cell wall, as well as the metabolisms of the molecules in the cell.

**Supplementary Materials:** The following are available online at <https://www.mdpi.com/article/10.3390/plants10102183/s1>, Figure S1: SDS Gels after expression and purification of DENV2, YFV, and WNV NS2B/NS3<sup>PRO</sup>, Figure S2: HST and HST inhibitory activity against DENV2, YFV, and WNV NS2B/NS3<sup>PRO</sup>, Figure S3: Fluorescence spectroscopy of Trp at 295 nm of DENV2, YFV, and WNV NS2B/NS3<sup>PRO</sup> in the presence of HST, Figure S4: Fluorescence spectroscopy of Trp at 295 nm of DENV2, YFV, and WNV NS2B/NS3<sup>PRO</sup> in the presence of HSD, Figure S5: Time dependent modifications of the DENV2 NS2B/NS3<sup>PRO</sup> structure, Figure S6: Time dependent modifications of the YFV NS2B/NS3<sup>PRO</sup> structure, Figure S7: Time dependent modifications of the WNV NS2B/NS3<sup>PRO</sup> structure, Figure S8: Time dependent modifications of the DENV2 NS2B/NS3<sup>PRO</sup>–HST complex, Figure S9: Time dependent modifications of the YFV NS2B/NS3<sup>PRO</sup>–HST complex, Figure S10: Time dependent modifications of the WNV NS2B/NS3<sup>PRO</sup>–HST complex, Figure S11: Time dependent modifications of the DENV2 NS2B/NS3<sup>PRO</sup>–HSD complex, Figure S12: Time dependent modifications of the YFV NS2B/NS3<sup>PRO</sup>–HSD complex, Figure S13: Time dependent modifications of the WNV NS2B/NS3<sup>PRO</sup>–HSD complex, Figure S14: 3D representation of NS2B/NS3<sup>PRO</sup>–HST and –HSD complex, Figure S15: Decomposition of the binding energy of DENV2 NS2B/NS3<sup>PRO</sup>–HST complex of two independent replica, Figure S16: Decomposition of the binding energy of YFV NS2B/NS3<sup>PRO</sup>–HST complex of two independent replica, Figure S17: Decomposition of the binding energy of WNV NS2B/NS3<sup>PRO</sup>–HST complex of two independent replica, Figure S18: Decomposition of the binding energy of DENV2

NS2B/NS3<sup>PRO</sup>-HSD complex of two independent replica, Figure S19: Decomposition of the binding energy of YFV NS2B/NS3<sup>PRO</sup>-HSD complex of two independent replica, Figure S20: Decomposition of the binding energy of WNV NS2B/NS3<sup>PRO</sup>-HSD complex of two independent replica, and Text S1: Expression and purification of NS2B/NS3 proteases.

**Author Contributions:** Conceptualization, R.J.E. and M.A.C.; methodology, R.J.E. and M.A.C.; software, D.S.O. and M.S.A.; validation, R.J.E., D.S.O. and M.A.C.; formal analysis, R.J.E. and M.A.C.; investigation, R.J.E., D.S.O. and M.A.C.; resources, M.S.A., D.W. and R.K.A.; writing—original draft preparation, R.J.E.; writing—review and editing, D.W., R.K.A. and M.A.C.; supervision, M.A.C. All authors have read and agreed to the published version of the manuscript.

**Funding:** This research was supported by grants from CNPq [Grant numbers 435913/2016-6, 401270/2014-9, 307338/2014-2], FAPESP [Grant numbers 2016/12904-0, 2018/12659-0, 2018/07572-3, 2019/05614-3], FUNDECT [23/200.307/2014], MOI III, CAPES, and PROPe UNESP. This study was supported in part by the UFMS/MEC-Brazil and UFT/MEC-Brazil.

**Institutional Review Board Statement:** Not applicable.

**Informed Consent Statement:** Not applicable.

**Data Availability Statement:** All data are reported in the text and Supplementary Materials.

**Acknowledgments:** We would like to thank the Institute of Biological Information Processing (Forschungszentrum Jülich, Germany) for their support.

**Conflicts of Interest:** The authors declare no conflict of interest. The funders had no role in the design of the study, in the collection, analyses, or interpretation of data, in the writing of the manuscript, or in the decision to publish the results.

## References

1. Badshah, S.L.; Faisal, S.; Muhammad, A.; Poulson, B.G.; Emwas, A.H.; Jaremko, M. Antiviral activities of flavonoids. *Biomed. Pharmacother.* **2021**, *140*, 111596. [\[CrossRef\]](#)
2. Wang, Y.; Chen, S.; Yu, O. Metabolic engineering of flavonoids in plants and microorganisms. *Appl. Microbiol. Biotechnol.* **2011**, *91*, 949–956. [\[CrossRef\]](#)
3. Hano, C.; Duangjai, T. Plant Polyphenols, more than Just Simple Natural Antioxidants: Oxidative Stress, Aging and Age-Related Diseases. *Medicines* **2020**, *7*, 26. [\[CrossRef\]](#)
4. Krych, J.; Lidia, G. Catalase is inhibited by flavonoids. *Int. J. Biol. Macromol.* **2013**, *58*, 148–153. [\[CrossRef\]](#)
5. Ragab, F.A.; Yahya, T.A.A.; El-Naa, M.M.; Arafa, R.K. Design, synthesis and structure–activity relationship of novel semi-synthetic flavonoids as antiproliferative agents. *Eur. J. Med. Chem.* **2014**, *82*, 506–520. [\[CrossRef\]](#) [\[PubMed\]](#)
6. Tian, S.S.; Jiang, F.S.; Zhang, K.; Zhu, X.X.; Jin, B.; Lu, J.J.; Ding, Z.S. Flavonoids from the leaves of *Carya cathayensis* Sarg. inhibit vascular endothelial growth factor-induced angiogenesis. *Fitoterapia* **2014**, *92*, 34–40. [\[CrossRef\]](#) [\[PubMed\]](#)
7. Zhang, X.; Huang, H.; Zhao, X.; Lv, Q.; Sun, C.; Li, X.; Chen, K. Effects of flavonoids-rich Chinese bayberry (*Myrica rubra* Sieb. et Zucc.) pulp extracts on glucose consumption in human HepG2 cells. *J. Funct. Foods* **2015**, *14*, 144–153. [\[CrossRef\]](#)
8. Garg, A.; Garg, S.; Zaneveld, L.J.D.; Singla, A.K. Chemistry and pharmacology of the Citrus bioflavonoid hesperidin. *Phytother. Res.* **2001**, *15*, 655–669. [\[CrossRef\]](#)
9. Ahmadi, A.; Hassandarvish, P.; Lani, R.; Yadollahi, P.; Jokar, A.; Bakar, S.A.; Zandi, K. Inhibition of chikungunya virus replication by hesperetin and naringenin. *RSC Adv.* **2016**, *6*, 69421–69430. [\[CrossRef\]](#)
10. Paredes, A.; Alzuru, M.; Mendez, J.; Rodríguez-Ortega, M. Anti-Sindbis activity of flavanones hesperetin and naringenin. *Biol. Pharm. Bull.* **2003**, *26*, 108–109. [\[CrossRef\]](#)
11. Eberle, R.J.; Olivier, D.S.; Pacca, C.C.; Avilla, C.M.S.; Nogueira, M.L.; Amaral, M.S.; Willbold, D.; Arni, R.K.; Coronado, M.A. In vitro study of Hesperetin and Hesperidin as inhibitors of zika and chikungunya virus proteases. *PLoS ONE* **2021**, *16*, e0246319. [\[CrossRef\]](#)
12. Morens, D.M.; Folkers, G.K.; Fauci, A.S. The challenge of emerging and re-emerging infectious diseases. *Nature* **2004**, *430*, 242–249. [\[CrossRef\]](#)
13. Mackenzie, J.S.; Gubler, D.J.; Petersen, L.R. Emerging flaviviruses: The spread and resurgence of Japanese encephalitis, West Nile and dengue viruses. *Nat. Med.* **2004**, *10*, S98–S109. [\[CrossRef\]](#)
14. Weissenböck, H.; Hubalek, Z.; Bakonyi, T.; Nowotny, N. Zoonotic mosquito-borne flaviviruses: Worldwide presence of agents with proven pathogenicity and potential candidates of future emerging diseases. *Vet. Microbiol.* **2010**, *140*, 271–280. [\[CrossRef\]](#)
15. Dobler, G. Zoonotic tick-borne flaviviruses. *Vet. Microbiol.* **2010**, *140*, 221–228. [\[CrossRef\]](#)
16. Gould, E.A.; Solomon, T. Pathogenic flaviviruses. *Lancet* **2008**, *371*, 500–509. [\[CrossRef\]](#)
17. Mukhopadhyay, S.; Kuhn, R.J.; Rossmann, M.G. A structural perspective of the flavivirus life cycle. *Nat. Rev. Microbiol.* **2005**, *3*, 13–22. [\[CrossRef\]](#)

18. Henschal, E.A.; Putnak, J.R. The dengue viruses. *Clin. Microbiol. Rev.* **1990**, *3*, 376–396. [CrossRef]
19. Falgout, B.; Pethel, M.; Zhang, Y.M.; Lai, C.J. Both nonstructural proteins NS2B and NS3 are required for the proteolytic processing of dengue virus nonstructural proteins. *J. Virol.* **1991**, *65*, 2467–2475. [CrossRef]
20. Lescar, J.; Luo, D.; Xu, T.; Sampath, A.; Lim, S.P.; Canard, B.; Vasudevan, S.G. Towards the design of antiviral inhibitors against flaviviruses: The case for the multifunctional NS3 protein from dengue virus as a target. *Antivir. Res.* **2008**, *80*, 94–101. [CrossRef]
21. Sampath, A.; Padmanabhan, R. Molecular targets for flavivirus drug discovery. *Antivir. Res.* **2009**, *81*, 6–15. [CrossRef]
22. Panche, A.N.; Diwan, A.D.; Chandra, S.R. Flavonoids: An overview. *J. Nutr. Sci.* **2016**, *5*, e47. [CrossRef] [PubMed]
23. Waldrop, G.L. A qualitative approach to enzyme inhibition. *Biochem. Mol. Biol. Educ.* **2009**, *37*, 11–15. [CrossRef] [PubMed]
24. Roy, A.; Lim, L.; Srivastava, S.; Lu, Y.; Song, J. Solution conformations of Zika NS2B-NS3pro and its inhibition by natural products from edible plants. *PLoS ONE* **2017**, *12*, e0180632. [CrossRef] [PubMed]
25. de Sousa, L.R.F.; Wu, H.; Nebo, L.; Fernandes, J.B.; Kiefer, W.; Kanitz, M.; Bodem, J.; Diederich, W.E.; Schirmeister, T.; Vieira, P.C. Flavonoids as noncompetitive inhibitors of Dengue virus NS2B-NS3 protease: Inhibition kinetics and docking studies. *Bioorg. Med. Chem.* **2015**, *23*, 466–470. [CrossRef] [PubMed]
26. Kiat, T.S.; Phippen, R.; Yusof, R.; Ibrahim, H.; Khalid, N.; Rahman, N.A. Inhibitory activity of cyclohexenyl chalcone derivatives and flavonoids of fingerroot, *Boesenbergia rotunda* (L.), towards Dengue-2 virus NS3 protease. *Bioorg. Med. Chem. Lett.* **2006**, *16*, 3337–3340. [CrossRef]
27. Hopkins, A.L.; Groom, C.R.; Alex, A. Ligand efficiency: A useful metric for lead selection. *Drug Discov. Today* **2004**, *9*, 430–431. [CrossRef]
28. Reynolds, C.H.; Bembenek, S.D.; Tounge, B.A. The role of molecular size in ligand efficiency. *Bioorg. Med. Chem. Lett.* **2007**, *17*, 4258–4261. [CrossRef] [PubMed]
29. Catici, D.A.; Amos, H.E.; Yang, Y.; van den Elsen, J.M.; Pudney, C.R. The red edge excitation shift phenomenon can be used to unmask protein structural ensembles: Implications for NEMO–ubiquitin interactions. *FEBS J.* **2016**, *283*, 2272–2284. [CrossRef]
30. Leung, D.; Schroder, K.; White, H.; Fang, N.X.; Stoermer, M.J.; Abbenante, G.; Martin, J.L.; Young, P.R.; Fairlie, D.P. Activity of recombinant dengue 2 virus NS3 protease in the presence of a truncated NS2B cofactor, small peptide substrates, and inhibitors. *J. Biol. Chem.* **2001**, *276*, 45762–45771. [CrossRef]
31. Gruba, N.; Rodriguez Martinez, J.I.; Grzywa, R.; Wysocka, M.; Skoreński, M.; Burmistrz, M.; Łęcka, M.; Lesner, A.; Sieńczyk, M.; Pyrc, K. Substrate profiling of Zika virus NS2B/NS3 protease. *FEBS Lett.* **2016**, *590*, 3459–3468. [CrossRef]
32. Mueller, N.H.; Yon, C.; Ganesh, V.K.; Padmanabhan, R. Characterization of the West Nile virus protease substrate specificity and inhibitors. *Int. J. Biochem. Cell Biol.* **2007**, *39*, 606–614. [CrossRef]
33. Motulsky, H.; Christopoulos, A. *Fitting Models to Biological Data Using Linear and Nonlinear Regression: A Practical Guide to Curve Fitting*; GraphPad Software, Inc.: San Diego, CA, USA, 2003.
34. Selvaraj, C.; Tripathi, S.K.; Reddy, K.K.; Singh, S.K. Tool development for Prediction of pIC<sub>50</sub> values from the IC<sub>50</sub> values—A pIC<sub>50</sub> value calculator. *Curr. Trends Biotechnol. Pharm.* **2011**, *5*, 1104–1109.
35. Coronado, M.A.; Eberle, R.J.; Bleffert, N.; Feuerstein, S.; Olivier, D.S.; de Moraes, F.R.; Willbold, D.; Arni, R.K. Zika virus NS2B/NS3 proteinase: A new target for an old drug—Suramin a lead compound for NS2B/NS3 proteinase inhibition. *Antivir. Res.* **2018**, *160*, 118–125. [CrossRef] [PubMed]
36. Johnson, M.L.; Frasier, S.G. Nonlinear least-squares analysis. *Meth. Enzymol.* **1985**, *117*, 301–342.
37. Shaikh, S.M.T.; Seetharamappa, J.; Ashoka, S.; Kandagal, P.B. A study of the interaction between bromopyrogallol red and bovine serum albumin by spectroscopic methods. *Dyes Pigment.* **2007**, *73*, 211–216. [CrossRef]
38. Wang, G.; Liu, X.; Yan, C.; Bai, G.; Lu, Y. Probing the binding of trypsin to glutathione-stabilized gold nanoparticles in aqueous solution. *Colloids Surf. B Biointerfaces* **2015**, *135*, 261–266. [CrossRef] [PubMed]
39. Ahumada, M.; Lissi, E.; Montagut, A.M.; Valenzuela-Henríquez, F.; Pacioni, N.L.; Alarcon, E.I. Association models for binding of molecules to nanostructures. *Analyst* **2017**, *142*, 2067–2089. [CrossRef]
40. Irwin, J.J.; Shoichet, B.K. ZINC—A free database of commercially available compounds for virtual screening. *J. Chem. Inf. Model.* **2005**, *45*, 177–182. [CrossRef]
41. Frisch, M.J.; Trucks, G.W.; Schlegel, H.B.; Scuseria, G.E.; Robb, M.A.; Cheeseman, J.R.; Scalmani, G.; Barone, V.; Mennucci, B.; Petersson, G.A.; et al. Gaussian, Inc., Gaussian 16, Revision B.01 n.d. Available online: <https://gaussian.com/> (accessed on 7 July 2021).
42. Wang, J.; Wang, W.; Kollman, P.A.; Case, D.A. Automatic atom type and bond type perception in molecular mechanical calculations. *J. Mol. Graph. Model.* **2006**, *25*, 247–260. [CrossRef]
43. Wang, J.M.; Wolf, R.M.; Caldwell, J.W.; Kollman, P.; Case, D. Development and testing of a general amber force field. *J. Comput. Chem.* **2004**, *25*, 1157–1174. [CrossRef]
44. Gordon, J.C.; Myers, J.B.; Folta, T.; Shoja, V.; Heath, L.S.; Onufriev, A. H++: A server for estimating pKas and adding missing hydrogens to macromolecules. *Nucleic Acids Res.* **2005**, *33* (Suppl. 2), W368–W371. [CrossRef]
45. Case, D.A.; Cerutti, D.S.; Cheatham, T.E., III; Darden, T.A.; Duke, R.E.; Giese, T.J.; Gohlke, H.; Goetz, A.W.; Greene, D.; Homeyer, N.; et al. AMBER; University of California: San Francisco, CA, USA, 2018.
46. Tian, C.; Kasavajhala, K.; Belfon, K.A.A.; Raguetta, L.; Huang, H.; Miguez, A.N.; Bickel, J.; Wang, Y.; Pincay, J.; Wu, Q.; et al. ff19SB: Amino-Acid-Specific Protein Backbone Parameters Trained against Quantum Mechanics Energy Surfaces in Solution. *J. Chem. Theory Comput.* **2020**, *16*, 528–552. [CrossRef] [PubMed]

47. Darden, T.; York, D.; Pedersen, L. Particle mesh Ewald: An  $N \cdot \log(N)$  method for Ewald sums in large systems. *J. Chem. Phys.* **1993**, *98*, 10089. [[CrossRef](#)]
48. Roe, D.R.; Cheatham, T.E., III. PTRAJ and CPPTRAJ: Software for processing and analysis of molecular dynamics trajectory data. *J. Chem. Theory Comput.* **2013**, *9*, 3084–3095. [[CrossRef](#)] [[PubMed](#)]
49. Case, D.A.; Cheatham, T.E., III; Darden, T.; Gohlke, H.; Luo, R.; Merz, K.M.; Onufriev, A.; Simmerling, C.; Wang, B.; Woods, R.J. The Amber biomolecular simulation programs. *J. Comput. Chem.* **2005**, *26*, 1668–1688. [[CrossRef](#)] [[PubMed](#)]
50. Nguyen, H.; Roe, D.R.; Simmerling, C. Improved Generalized Born Solvent Model Parameters for Protein Simulations. *J. Chem. Theory Comput.* **2013**, *9*, 2020–2034. [[CrossRef](#)]